Biomed Microdevices
DOI 10.1007/s10544-008-9217-0

Capture and alignment of *phi29* viral particles in sub-40 nanometer porous alumina membranes

Jeong-Mi Moon · Demir Akin · Yi Xuan · Peide D. Ye · Peixuan Guo · Rashid Bashir

Abstract Bacteriophage phi29 virus nanoparticles and its associated DNA packaging nanomotor can provide for novel possibilities towards the development of hybrid bio-nano structures. Towards the goal of interfacing the phi29 viruses and nanomotors with artificial micro and nano-structures, we fabricated nanoporous Anodic Aluminum Oxide (AAO) membranes with pore size of 70 nm and shrunk the pores to sub 40 nm diameter using atomic layer deposition (ALD) of Aluminum Oxide. We were able to capture and align particles in the anodized nanopores using two methods. Firstly, a functionalization and polishing process to chemically attach the particles in the inner surface of the pores was developed. Secondly, centrifugation of the particles was utilized to align them in the pores of the nanoporous membranes. In addition, when a mixture of empty capsids and packaged particles was centrifuged at specific speeds, it was found that the empty capsids deform and pass through 40 nm diameter pores whereas the particles packaged with DNA were mainly retained at the top surface of the nanoporous membranes. Fluorescence microscopy was used to verify the selective filtration of empty capsids through the nanoporous membranes.

Keywords *phi29* · Nanoporous membrane · Atomic layer deposition · Alignment · Capture

J.-M. Moon · Y. Xuan · P. D. Ye
Birck Nanotechnology Center, School of Electrical and Computer Engineering, Purdue University,
West Lafayette, IN 47907, USA

D. Akin
Birck Nanotechnology Center,
Weldon School of Biomedical Engineering, Purdue University,
West Lafayette, IN 47907, USA

P. Guo
School of Biomedical Engineering, University of Cincinnati,
Cincinnati, OH 45221, USA

R. Bashir (✉)
Micro and Nanotechnology Laboratory, Department of Electrical and Computer Engineering and Bioengineering,
University of Illinois at Urbana-Champaign,
Urbana, IL 61801, USA
e-mail: rbashir@uiuc.edu

Present address:
J.-M. Moon
Micro and Nanotechnology Laboratory,
Department of Electrical and Computer Engineering,
University of Illinois at Urbana-Champaign,
Urbana, IL 61801, USA

Present address:
D. Akin
Center for Cancer Nanotechnology Excellence,
Stanford University School of Medicine,
The James H. Clark Center,
Stanford, CA 94305-5427, USA

1 Introduction

Viruses are masterpieces of nanoengineering designed as replicating machines. The novelty and ingenious design of these biological nanomachines can help inspire the development of biomimetics for nanodevices. For instance, the bacteriophage *phi29* contains a switchable DNA-packaging motor that has been shown to be one of the most powerful biomotors studied so far (Shu and Guo 2003a). This nanomotor is driven by six ATP-binding pRNA molecules that bind to the connector protein, as schematically shown in Fig. 1 (Guo et al. 1991; Shu and Guo 2003b). Conformational changes and sequential action

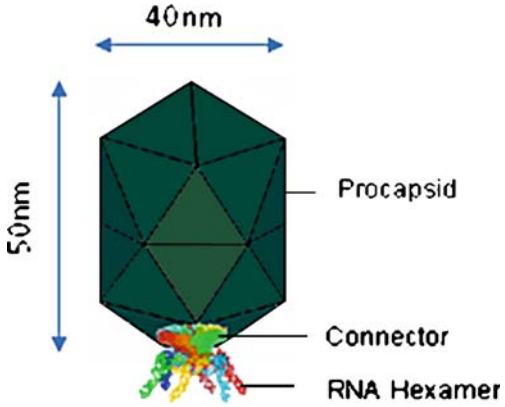

Fig. 1 Schematic of a *phi29* viral particle. The particle size is about 40×50 nm and contains a DNA packaging nanomotor at one end

of the pRNA ensure the motor rotates continuously, using ATP as the energy source to package DNA molecules that are up to 20,000 base pairs or 6 μm in length (Zhang et al. 1998; Chen and Guo 1997; Guo et al. 1998; Chen et al. 1999; Guo et al. 1987). This packaging process involves a delicate balance of forces which are both mechanical and electrostatic in nature (Klug et al. 2005). The motor of *phi29* can generate a force of up to 57 pN (Smith et al. 2001). Such a force is enough to pump DNA against the high internal pressure that builds up as the viral DNA is packed inside the capsid.

For the separation, collection, and filtration of viruses, membrane-based technologies have been developed as useful and efficient methods (Lakshmi and Martin 1997; van Reis and Zydney 2001; Xu et al. 2005; Yang et al. 2006; Lee et al. 2002). Potentially, membranes are well adapted for these applications because their pore size and surface chemistry can be adjusted to the size and surface chemistry of an organism of interest, and the specific capture (selective sensing) of this organism could be possible. Several types of membranes have been employed for virus capture and separation; however, many of these have not been effective (van Voorthuizen et al. 2001; Otaki et al. 1998; Urase et al. 1996). For example, in case of microfiltration membranes, the pore size is typically much larger than the size of the virus particles that are tens of nanometers in size (van Voorthuizen et al. 2001; Otaki et al. 1998). The smaller pore size ultramembranes have uneven distribution of pore size, allowing virus particles to permeate into a small number of abnormally large pores (Urase et al. 1996). Although chemically specific filtration using nanoporous membranes has been shown for small molecules (Jirage et al. 1999; Lee and Martin 2001; Fernandez-Lopez et al. 2001; Chun and Stroeve 2002), specific bio-organism immobilization, capture, and detection remain to be a great technical challenge.

2 Experimental

2.1 Material and reagents

High-purity Al foil (99.999%, 0.2 in. thickness) was purchased from Research and PVD Materials. Trimethylaluminum (TMA) and 3-(trimethoxysilyl)propyl aldehyde (TMSPA) were purchased from Aldrich and used without further purification. Deionized water was obtained from an ultrafiltration system (Milli-Q, Millipore) with a measured resistivity above 18 MΩcm and passed through a 0.22 μm filter to remove particulate matter.

2.2 Fabrication of nanoporous AAO membrane

Aluminum foil was first anodized in a 0.3 M oxalic acid solution at 5°C at a constant applied voltage of 40 V for 20 h and then etched in an aqueous mixture of 6 wt % phosphoric acid and 1.8 wt % chromic acid at 60°C. A second anodization was performed for 8 h using the same conditions as above, followed by dissolution of the remaining Al in a saturated $HgCl_2$ solution. Pore widening and removal of the barrier oxide layer were carried out by chemical etching in 0.8 wt % phosphoric acid at 30°C for 60 min to produce AAO membranes with highly ordered pores (diameter=75 nm, center-to-center distance=105 nm), as shown in Fig. 2(a) and (b). The final thickness of the membrane was 24 μm with pores across the membranes.

2.3 Atomic layer deposition

We used an ASM F-120 ALD system for shrinking the pore size of AAO membrane. ALD Al_2O_3 films were deposited by using alternating pulse of trimethylaluminum (TMA) [$Al(CH_3)_3$] and water (H_2O) precursors. H_2O vapor was used to oxidize chemisorbed TMA. N_2 was used as a carrier gas to transport precursor vapor to the membrane surface and purge reaction gases from the reactor during each half-reaction. The pulse time of TMA, H_2O and N_2 were 0.8 s, 1.2 s and 2.0 s, respectively. For our purpose, the deposition process was run for 133 to 211 cycles at 2–5 Torr at 300°C and the growth rate was 0.9 Å per cycle for Al_2O_3.

2.4 Array of *phi29* procapsid on the alumina membranes

3% 3-(trimethoxysilyl)propyl aldehyde (TMSPA) solution was prepared in ethanol/H_2O (95%/5%) and membranes were immersed to clean the ALD/AAO membrane for 3 h. After washing the aldehyde-silanized ALD/AAO with ethanol several times, the membranes were dried in a stream of nitrogen gas and heated at 110°C for 20 min. The aldehyde-silanized alumina membrane was incubated in a

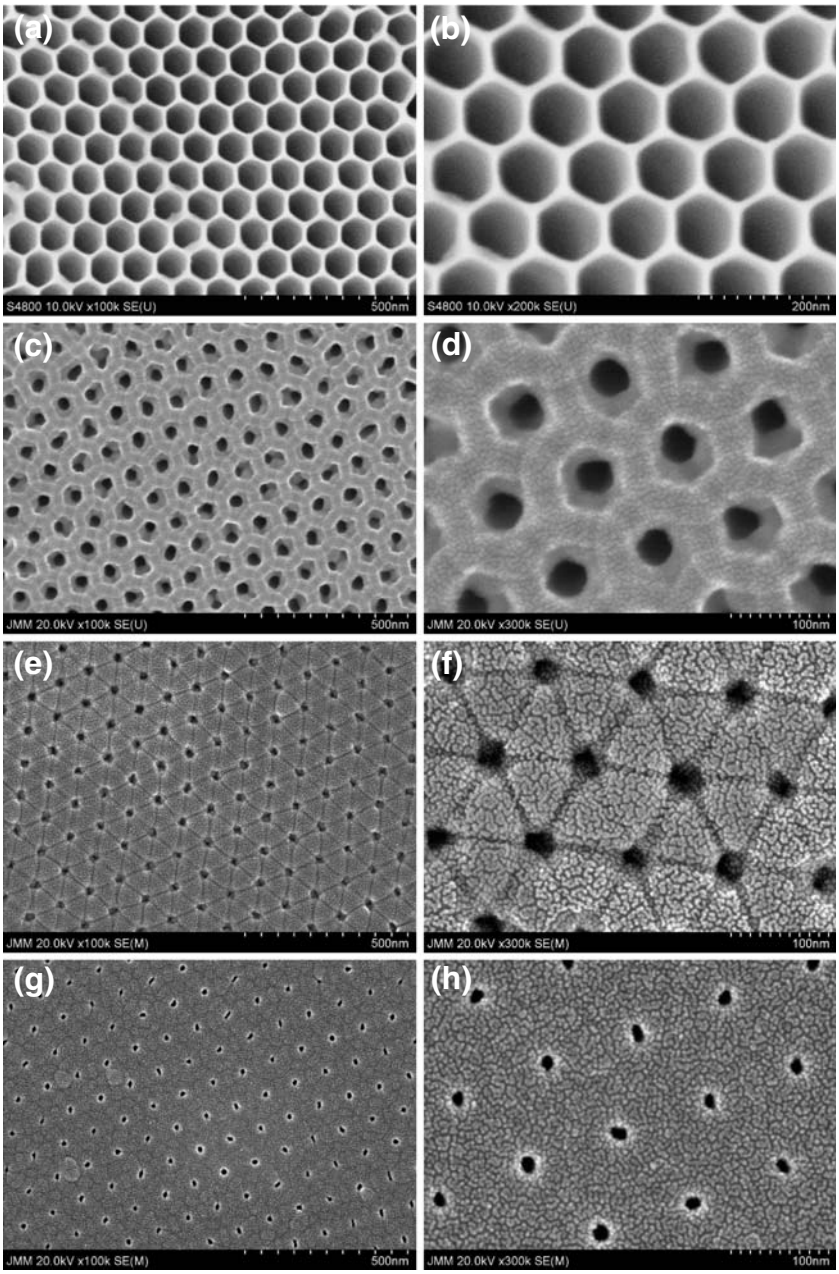

Fig. 2 Field-emission scanning electron microscope (FE-SEM) images of the anodic aluminum oxide (AAO) membranes and further shrunk by atomic-layer deposition (ALD). The images show the shrunk pore sizes; (**a**) and (**b**) 75±5 nm as anodized nanoporous membranes, (**c**) and (**d**) 39±4 nm, (**e**) and (f) 25± 3 nm, and (**g**) and (**h**) 15±1 nm

solution of procapsid (without pRNA; 0.01 mg/mL in TMS buffer) for 15 h at room temperature. The membrane was then immersed into fresh TMS buffer for 30 min. at room temperature to remove any unattached procapsids.

2.5 Procedure for the DNA-packaging of *phi29 in vitro*

Briefly, 1 μg of RNA in 1 μL RNase free H_2O was mixed with 10 μL of purified procapsids (0.4 mg/ml) in TMS (100 mM NaCl, 10 mM $MgCl_2$, 50 mM Tris, pH 7.8) and then incubated for 60 min at room temperature. The pRNA-enriched procapsids were then mixed with 3 μL of ATP (10 mM in TMS), 6 μL of gp16 (0.5 mg/mL), and 1 μL of DNA-gp3 (200 ng/μL) and incubated 60 min at room temperature to complete the DNA-packaging reaction. We used these DNA-packaged *phi29* particles for the experiments described in subsequent sections.

3 Results and discussion

In this paper, we report the use of anodized aluminum oxide (AAO) membranes with narrow pore size distribution and chemically modifiable surfaces for alignment and

capture of *phi29* particles. Highly ordered nanoporous AAO membranes were prepared by a two-step anodization process similar to described above and also previously (Moon and Wei 2005), resulting in structures as shown in Fig. 2(a) and (b).

The nanopores of these AAO films are still big compared to the *phi29* nanomotors. Next, we decreased the pore sizes using atomic layer deposition (ALD) which significantly shrinks but does not fully seal the nanopores (Xiong et al. 2005; Miikkulainen et al. 2008). ALD is a promising technique to form ultrathin films uniformly over a large wafer and 3-D structures such as deep trenches and deep holes with atomic-scale thickness controllability. ALD consists of two half reactions: (1) self-limiting chemisorption of metal-organic or metal-halide precursor on the wafer surface and (2) reaction of the chemisorbed these species with oxygen-containing species such as water vapor, O_2, O_3, or metal alkoxide. Generally ALD-growth is carried out at a relative low temperature (ca. 300°C) because thermal decomposition of precursor at higher temperatures deteriorates the thickness controllability. After the ALD process was completed, field-emission scanning electron microscope (FE-SEM; Hitachi S-4800) analysis of nanoporous ALD/AAO membranes revealed pore diameters on the order of 39 nm, 25 nm, and 15 nm, respectively, with increasing times used for the deposition (Fig. 2(c)–(h)).

To use the ALD/AAO membranes for the biochemically assisted self-assembly, biomolecules need to be attached to the surface of the alumina membrane. The experimental procedure of the immobilization on the membrane surface and hybridization of bio-nano structures is schematically shown in Fig. 3(a). The procapsid of *phi29* is formed by self assembly via protein–protein interactions of the scaffolding protein gp7, the capsid protein gp8, and the portal vertex protein gp10 (Lee and Guo 1995). The procapsids contain a connector (or portal vertex) with 12 protein subunits, a circular oligomer with a central tunnel through which the DNA is translocated into the procapsid during the assembly process or ejected out of the mature capsid during the host cell infection. Figure 3(b) and (c) shows tunneling electron microscopy (TEM, Philips C-100) images of negative-stained procapsids with an average diameter of 45 nm as well as unreacted connectors with an average diameter of 14 nm. These connectors could be removed with further purification of the samples.

For the array of procapsid on the alumina membranes, 3-(trimethoxysilyl)propyl aldehyde (TMSPA), was used as a bi-functional modifier to functionalize the AAO membrane. This is possible since the silane groups can form covalent bonds with the Aluminum Oxide (Al_2O_3) surfaces and the amine groups of procapsid can be attached to the aldehyde groups on the membranes. First, the membrane surface (39 nm pore diameter) was modified with TMSPA. The aldehyde-silanized alumina membrane was then incubated in a solution of procapsid (without pRNA). The morphology of biomaterial particles on the ALD/AAO was

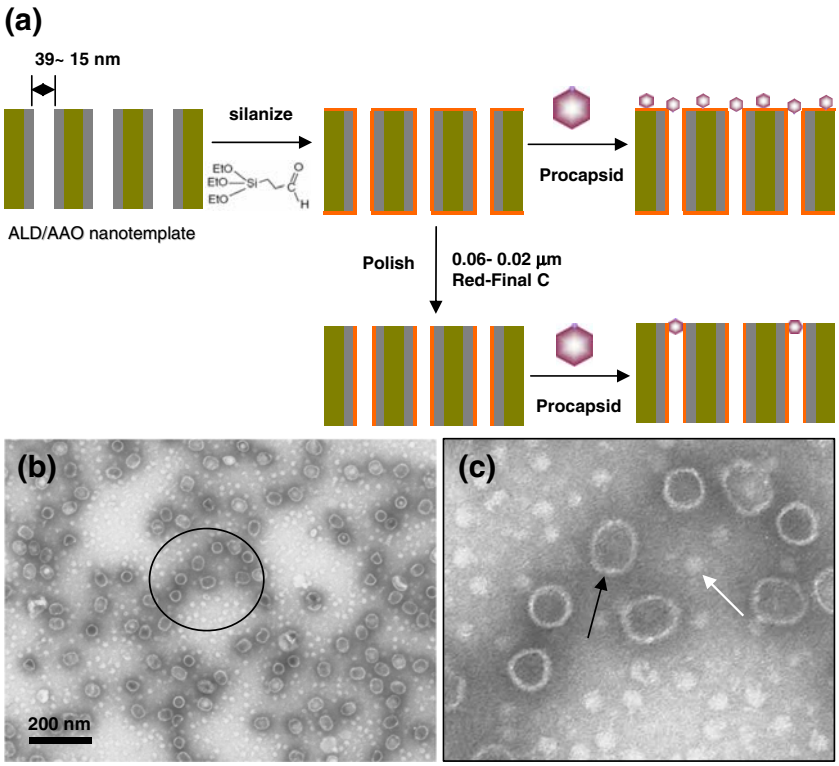

Fig. 3 (**a**) Schematic depiction of the experimental procedure, (**b**) transmission electron microscopy (TEM) of the empty *phi29* procapsids, (**c**) expanded view of the region in dashed circle in (**b**) to show the empty procapsid particles (*black arrow*) and the connectors (*white arrow*)

characterized by field-emission scanning electron microscope (FE-SEM; Hitachi S-4800). Metal Au/Pd film was sputter deposited on the surface of biomaterials for FE-SEM samples. Binding of procapsid particles both in the pores and on the top surface of the membrane with MPTMS are shown in the FESEM images in Fig. 4(a) and (b). The particles have an average size of 30 nm as shown in Fig. 4(c). The large size distribution is attributed to a mixture of procapsid and individual connector particles in the solution.

In order to attach the biomaterial particles to the pores only and not to the top surface, the aldehyde-silanized ALD/AAO membranes were polished for 10 s with 0.06 μm polishing cloth (Red-Final C; Allied High Tech Products) to remove the aldehyde-silanized layer from the face of the alumina surface. After polishing, the membrane was placed into a solution containing 0.01 mg/ml of procapsid dispersed in the TMS buffer for 4 h. The resulting FESEM images in Fig. 4(d, e) show that indeed the particles were mostly attached in the pores. The histogram in Fig. 4(f) represents the quantity of particles attached to the membranes. The unpolished membrane shows that 50% of the biomaterial particle binding occurred in the pores and 50% out of the pores. In contrast, the polished membrane shows particle binding to be localized at about 84% in the pores and about 16% out of the pores.

For the size selective capture of biomaterial onto ALD/AAO membranes, we also filtered the solution with the *phi29* particles by centrifugation. The membrane pore size can be adjusted to smaller than that of a biomaterial particle allowing the specific capture of this particle of interest. To investigate this hypothesis, we decreased the pores to 38 nm on as-prepared AAO substrates using the ALD method. First, we tested the ability of the membranes to capture empty procapsids. Then, we attempted to use DNA-packaged *phi29* particles with the nanoporous ALD/AAO membranes. The procedure for the DNA-packaging of *phi29 in vitro* was used as described in the earlier section and previously (Lee and Guo 1995). Figure 5(a, b) shows the TEM images, negatively stained, of the DNA filled

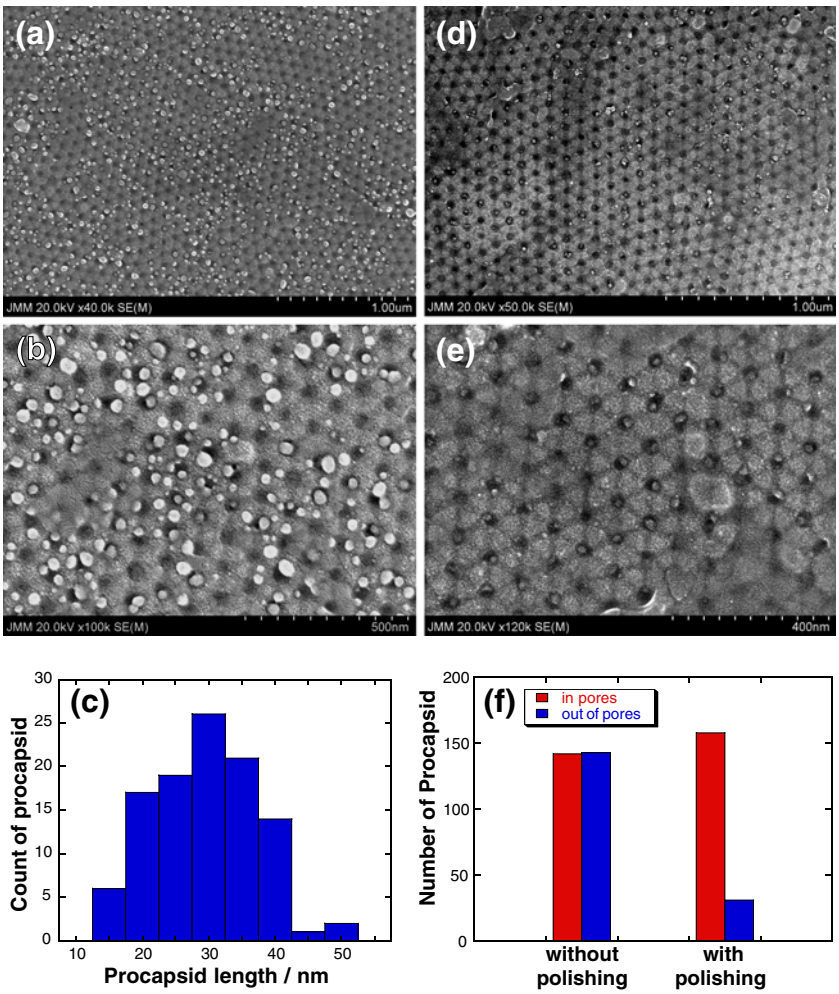

Fig. 4 (**a** and **b**) Field-emission scanning electron microscope (FE-SEM) images of the empty *phi29* particle binding to an unpolished ALD/AAO membrane. (**c**) graph showing the average size of the empty particle being 30 nm. The large size distribution could be attributed to a mixture of procapsid, protein fragments, and individual connector particles in the solution. (**d** and **e**) FE-SEM images of the empty *phi29* particle binding to a polished membranes. (**f**) Histogram showing that particle binding to the unpolished membrane occurs 50% in the pores and 50% out of the pores. In contrast, the particle binding to the polished membrane results in 84% in the pores and 16% out of the pores

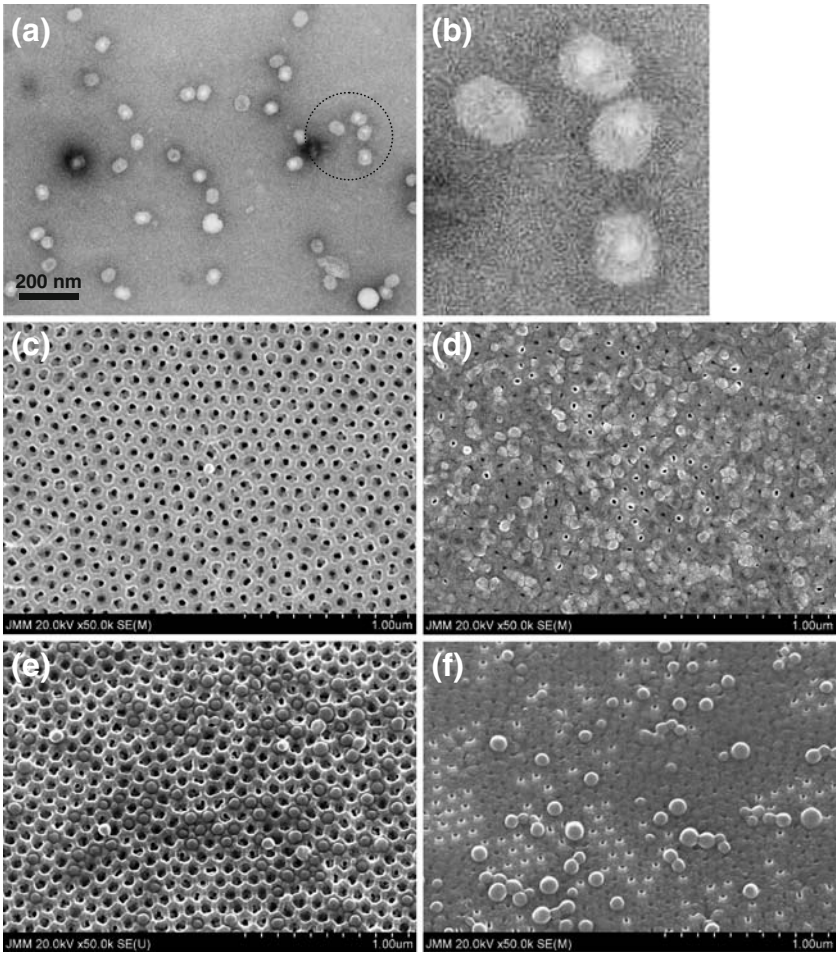

Fig. 5 (**a**) Transmission electron microscopy (TEM) of the DNA filled *phi29* capsids, (**b**) Expanded view of the region in dashed circle in (**a**) to show the DNA packaged particles. Note the difference in contrast between the empty and filled particles. The packaged capsids have greater electron density resulting in clearer contrast. Field-emission scanning electron microscope (FE-SEM) images of the top (**c**) and bottom (**d**) of the ALD/AAO membrane after centrifugation with empty procapsids. As can be noted, very few particles remain on the top surface and most of the particles have passed through and are retained on the bottom side. Field-emission scanning electron microscope (FE-SEM) images of the top (**e**) and bottom (**f**) of the ALD/AAO membrane after centrifugation with DNA filled capsids. More particles are retained on the top which do not pass through

phi29 capsids. In clear contrast to the TEM images of the empty procapsids, the regions inside the particles appear dense and brighter for the packaged capsids. We then performed filtration experiments in a modified swinging bucket centrifuge (Eppendorf 5804) at 1680 x g (3000 rpm) for 5 min. The empty procapsid particles penetrated through the ALD/AAO membrane pores and were retained on the bottom surface of the membrane, as shown in Fig. 5(c) (top surface) and (d) (bottom surface). This novel result is particularly interesting considering that the membrane pores (~38 nm) are smaller than the procapsid particles (average diameter of ~ 45 nm). However, lots of particles were observed on the top side of membranes for the case of the packaged capsid particles filtered through the ALD/AAO membrane (Fig. 5(e), (f)).

To identify and also characterize their DNA encapsulation status, the particles found on both sides of the membrane in the Fig. 5(e) and (f), top and bottom, respectively, were dual stained with DiI (stains proteins fluorescent red) and YoYo-1 (stains DNA fluorescent green-blue) according to an already published protocol (Akin et al. 2004), followed by fluorescence image acquisition of both surfaces using a color, cooled CCD camera (Fig. 6(a), (b)). As seen in the Fig. 6(a) (top side) and (b) (bottom side), the top surface showed yellow co-localization signal of fluorescent green to light blue labeled DNA and fluorescent red *phi29* procapsid. In contrast, the bottom surface showed mainly the red-labeled empty procapsid particles and green to light blue DNA as separate components. Further analysis of the RGB channels of Fig. 6(a) and (b) was done by plotting the intensity profiles of each color channel of the top (Fig. 6(c)) and the bottom (Fig. 6(d)) of the membranes. The resulting separate color channel intensities of the top and the bottom surfaces were quantified (Fig. 6(e)) and it was found that the majority of the DNA (green) was retained within the capsids (red) located at the top surface. Some DNA fluorescence was also observed in the images acquired from the bottom side indicating the possible existence of partially filled capsids or free DNA since these could also pass through the pores. These results indicate that the nanoporous ALD/AAO membranes with appropriate centrifugation conditions

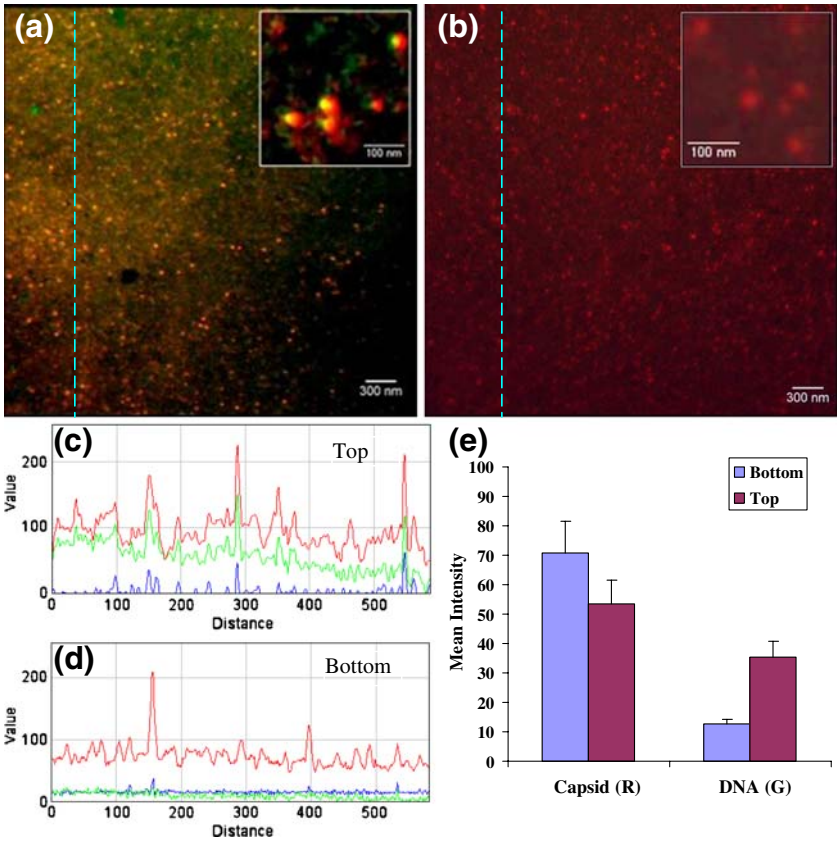

Fig. 6 Fluorescence images of *phi29* capsids on top side (**a**) and the bottom side (**b**) of the membrane after the centrifugation process. High resolution view of the fluorescence image is shown in the *inset* of (**a**) and (**b**), respectively. The top surface shows yellow co-localization signal of fluorescent green to light blue labeled DNA and fluorescent red capsid. In contrast, the bottom surface shows mainly the red-labeled empty procapsid particles. Average intensity values for each of the RGB channels of the top surface (**c**) and the bottom surface are shown in (**d**) as extracted from the line profile plots (*blue lines* in **a** and **b**). Quantification of the locations of red fluorescent capsid and green fluorescent DNA are shown in (**e**). Majority of the DNA-containing capsids are found on the top surface, however, some partially packaged capsids are also evident at the bottom surface as indicated by the observation of green fluorescence signal at the bottom surface

could be used for discrimination of *phi29* particles with and without fully packaged DNA from a mixture and this novel method may be of use for the determination of DNA packaging rate as an alternate method to plaque/infectivity titration based methods.

We suggest that the empty procapsid undergoes structural changes due to centrifugal force (1680 x g) during the centrifugation based filtering. The capsids have thin walls compared to their diameters, for example, the wall thickness of the *phi29* capsid is ~1.5 nm, whereas its linear dimensions are on the order of 40–50 nm (Tao et al. 1998). Moreover, the protein: protein interactions within the empty procapsids may not be fully stabilized. These factors might allow the empty procapsid the flexibility to deform sufficiently to traverse through a pore smaller than its own physical dimensions.

Many important and also related aspects of bacteriophage *phi29* morphogenesis and mechanoelastic properties have not been fully investigated yet. One of these aspects is the influence of the enclosed viral DNA on the mechanical properties of the viral particle and its stability. The prohead of *phi29* has 10 hexameric units in its cylindrical equatorial region, and 11 pentameric and 20 hexameric units comprise icosahedral end-caps with $T=3$ quasi-symmetry (Tao et al. 1998). In a recent study, under identical conditions, the comparison of the spring constants of the empty capsid and the viron of minute virus of mice (MVM), known to have icosahedral ($T=1$) symmetry, showed that the presence of the genomic DNA leads to an increase of the particle stiffness by 3%, 42%, and 140% when probed along fivefold, threefold, and twofold symmetry axes, respectively (Carrasco et al. 2006). The DNA molecule could reinforce the particle by coating the internal surface of the capsid, thus increasing the effective capsid wall thickness homogeneously. By structural analogy, we believe this phenomenon may also explain why DNA-packaged *phi29* did not traverse the AAO membrane pores in our case; however, more detailed studies are needed to fully characterize this effect.

4 Conclusions

Our studies lay the ground work for interfacing viral nanoparticles with the nanoporous AAO membranes. We used atomic-layer deposition to precisely shrink the pore size of the nanoporous alumina membranes down to 15 nm. In addition, the alignment of viral particles on the pores was demonstrated either by chemical functionalization and polishing or by a centrifugation process. In particular, the nanoporous ALD/AAO membranes can also be used to separate fully DNA-packaged and unpackaged *phi29* particles from a mixture by the centrifugation method. The centrifugation while using the nanoporous membranes can be used for the filtration, purification, and concentration of various viruses.

Acknowledgments We acknowledge the funding from the National Institutes of Health through the NIH Roadmap for Medical Research (PN2 EY 018230 Nanomedicine Development Center), and NIH R21 EB007474 FE-SEM images were taken at the Birck Nanotechnology Center Microscopy Facility. We also thank Dr. D. Sherman for the TEM micrographs.

References

D. Akin, H. Li, R. Bashir, Nano Lett **4**, 257 (2004), doi:10.1021/nl034987p

C. Carrasco, A. Carreira, I.A.T. Schaap, P.A. Serena, J. Gomez-Herrero, M.G. Mateu et al., Proc. Natl. Acad. Sci. U S A **103**, 13706 (2006), doi:10.1073/pnas.0601881103

C. Chen, P. Guo, J. Virol **71**, 495 (1997)

C. Chen, C. Zhang, P. Guo, RNA **5**, 805 (1999), doi:10.1017/S1355838299990350

K.-Y. Chun, P. Stroeve, Langmuir **18**, 4653 (2002), doi:10.1021/la011250b

S. Fernandez-Lopez, H.-S. Kim, E.C. Choi, M. Delgado, J.R. Granja, A. Khasanov et al., Nature **412**, 452 (2001), doi:10.1038/35086601

P. Guo, S. Erickson, D. Anderson, Science **236**, 690 (1987), doi:10.1126/science.3107124

P. Guo, B. Rajogopal, D. Anderson, S. Erickson, C.-S. Lee, Virology **185**, 395 (1991), doi:10.1016/0042-6822(91)90787-C

P. Guo, C. Zhang, C. Chen, K. Garver, M. Trottier, Mol. Cell **2**, 149 (1998), doi:10.1016/S1097-2765(00)80124-0

K.B. Jirage, J.C. Hulteen, C.R. Martin, Anal. Chem **71**, 491 (1999), doi:10.1021/ac990615i

W.S. Klug, M.T. Feldmann, M. Ortiz, Comput. Mech **35**, 146 (2005), doi:10.1007/s00466-004-0613-x

B.B. Lakshmi, C.R. Martin, Nature **388**, 758 (1997), doi:10.1038/41978

C.-S. Lee, P. Guo, J. Virol **69**, 5018 (1995)

S.B. Lee, C.R. Martin, Chem. Mater **13**, 3236 (2001), doi:10.1021/cm0101071

S.B. Lee, D.T. Mitchell, L. Trofin, T.K. Nevanen, H. Söderlund, C.R. Martin, Science **296**, 2198 (2002), doi:10.1126/science.1071396

V. Miikkulainen, T. Rasilainen, E. Puukilainen, M. Suvanto, T.A. Pakkanen, Langmuir **24**, 4473 (2008), doi:10.1021/la800285s

J.-M. Moon, A. Wei, J. Phys. Chem. B **109**, 23336 (2005), doi:10.1021/jp054405n

M. Otaki, K. Yano, S. Ohgaki, Water Sci. Technol **37**, 107 (1998), doi:10.1016/S0273-1223(98)00300-X

D. Shu, P. Guo, Virology **309**, 108 (2003a), doi:10.1016/S0042-6822(03)00011-4

D. Shu, P. Guo, J. Biol. Chem **278**, 7119 (2003b), doi:10.1074/jbc.M209895200

D.E. Smith, S.J. Tans, S.B. Smith, S. Grimes, D.L. Anderson, C. Bustamante, Nature **413**, 748 (2001), doi:10.1038/35099581

Y. Tao, N.H. Olson, W. Xu, D.L. Anderson, M.G. Rossmann, T.S. Baker, Cell **95**, 431 (1998), doi:10.1016/S0092-8674(00)81773-0

T. Urase, K. Yamamoto, S. Ohgaki, J. Membr. Sci **115**, 21 (1996), doi:10.1016/0376-7388(95)00269-3

R. van Reis, A. Zydney, Curr. Opin. Biotechnol **12**, 208 (2001), doi:10.1016/S0958-1669(00)00201-9

E.M. van Voorthuizen, N.J. Ashbolt, A.I. Schäfer, . J. Membr. Sci **194**, 69 (2001), doi:10.1016/S0376-7388(01)00522-1

G. Xiong, J.W. Elam, H. Feng, C.Y. Han, H.-H. Wang, L.E. Iton et al., J. Phys. Chem. B **109**, 14059 (2005), doi:10.1021/jp0503415

Y. Xu, K.K. Sirkar, X.-P. Dai, R.G. Luo, . Biotechnol. Prog **21**, 590 (2005), doi:10.1021/bp049801m

S.Y. Yang, I. Ryu, H.Y. Kim, J.K. Kim, S.K. Jang, T.P. Russell, . Adv. Mater **18**, 709 (2006), doi:10.1002/adma.200501500

F. Zhang, S. Lemieux, X. Wu, D. St.-Arnaud, C.T. McMurray, F. Major et al., Mol. Cell **2**, 141 (1998), doi:10.1016/S1097-2765(00)80123-9